Rate-dependent modelling of concrete fracture

L. J. SLUYS and R. DE BORST
Delft University of Technology
Department of Civil Engineering

Abstract

Rate dependence is shown to introduce an internal length scale into initial value problems. As a result, solutions of initial value problems that involve softening no longer exhibit excessive mesh dependence. Numerical results have been obtained for one-dimensional localisation problems and for tensile tests on specimens with notches.

1 Introduction

To carry out proper transient failure analyses of concrete structures it is important to examine cracking and strain localisation in cracked zones. In a cracked section there is a decrease in the capacity to transmit tensile forces. This phenomenon is commonly called softening and is accompanied by the formation of narrow bands of intense straining. Mapping of measured load-displacement data onto stress-strain relations leads to a negative slope in the stress-strain curve. A numerical description of strain localisation reveals a severe dependence on the fineness of the mesh.
Recent studies (Read and Hegemier 1984, Sandler 1984, Lasry and Belytschko 1988) have clarified the mathematical background to the mesh-sensitivity problem. The field equations which describe the dynamic motion of the body lose hyperbolicity as soon as softening occurs. This means that the wave speeds become imaginary and consequently a non-physical solution is obtained in transient localisation problems. Solutions of initial value problems that involve softening (Bazant and Belytschko 1985) show localisation zones of zero thickness with infinite strains which develop in a time span that approaches zero. Numerical simulation of a softening solid exhibits the same features upon mesh refinement (Sluys 1989a). Strain localisation occurs in a zone the width of which is entirely determined by the element size. Energy dissipation in the fracture zone tends to zero upon mesh refinement, while the extent of wave reflection on cracks depends on the discretisation of a structure.
Three types of methods have been suggested in the literature to correct the above-mentioned deficiencies. The first class of methods consists of non-local models (Pijaudier-Cabot and Bazant 1987) and gradient models (Schreyer and Chen 1986, De Borst and Mühlhaus 1991, Mühlhaus and Aifantis 1991) in which higher-order displacement gradients are introduced in the material equations. A second approach is the micro-polar or Cosserat theory which allows mesh-objective analyses to be carried out under mode-II and mixed-mode conditions. This holds true for static (De Borst 1990, Mühlhaus, De Borst and Aifantis 1991) as well as dynamic loading conditions (Sluys

and De Borst 1990, Sluys 1990). The solution strategy followed here is based on the inclusion of the strain rate in the constitutive equations (Needleman 1988, Wu and Freund 1984). First, a rate-dependent model is treated and then numerical analyses with the model are described and attention is paid to the performance of the model with respect to mesh dependence.

2 Rate-dependent crack model

Rate dependence is introduced to prevent the character of the set of equations that describes the dynamic motion of the softening solid from becoming elliptic. The dynamic equations should possess real characteristics in the x-t plane. This is only possible if the initial value problem is not elliptic. Then well-posedness of the initial value problem is preserved and meaningful results can be obtained for localisation zones of intense straining. Because failure modes are usually accompanied by high strain rates the inclusion of the strain rate in the constitutive equations seems natural. For the solution of the mesh-sensitivity problem it is essential that rate dependence naturally introduces an internal length scale into the initial value problem, although the constitutive equations do not contain a parameter with the dimension of length. For the rate-dependent model treated here it will be proved that the initial value problem preserves well-posedness. The model has been implemented within the framework of the fixed smeared crack concept (De Borst and Nauta 1985, Rots 1988). In this concept a cracked zone is conceived to be a continuum which permits a description in terms of stress-strain relations.
A crack model that exhibits both softening and strain rate dependence is chosen according to

$$\sigma = f(\varepsilon_{cr}) + M_1 \dot{\varepsilon}_{cr}, \tag{1}$$

where σ and ε_{cr} denote stress and crack strain respectively, a superimposed dot denotes differentiation with respect to time, $f(\varepsilon_{cr})$ is a softening function and M_1 is the rate-sensitivity parameter. Note that rate dependence is chosen as a function of the inelastic strain ε_{cr} and not of the total strain. When a linear softening model is utilised as in this study

$$f(\varepsilon_{cr}) = f_t + D_1 \varepsilon_{cr} \tag{2}$$

eq.(1) becomes

$$\sigma = f_t + D_1 \varepsilon_{cr} + M_1 \dot{\varepsilon}_{cr}. \tag{3}$$

In eqs. (2) and (3) f_t is the initial tensile strength under static loading conditions and D_1 is a constant softening modulus. In the reference calculations the parameters have been chosen as: Young's modulus $E = 25000\ \mathrm{N/mm^2}$, $D_1 = -6000\ \mathrm{N/mm^2}$, $M_1 = 10\ \mathrm{Ns/mm^2}$ and $f_t = 3.0\ \mathrm{N/mm^2}$.
In Fig. 1 computed stress-strain curves are shown for various imposed strain rates. The curves show an increase of the tensile strength under dynamic loading, which is also

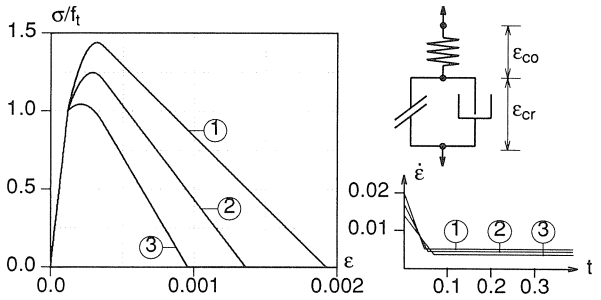

Fig. 1. Linear rate-dependent crack model: Left: Stress-strain curves for different imposed strain rates. Top right: Schematic representation of the model. Bottom right: Imposed strain rates.

observed in several experiments (Körmeling 1986, Zielinski 1982). In these experiments the increase of tensile strength f_t is measured as a function of a constant strain rate. However, both these tests and the numerical simulations described in the subsequent section show that the strain rate not only varies in time but also displays large gradients along the localisation zone. It is therefore difficult to derive the material rate sensitivity parameter M_1 from experimental data. As regards the increase of fracture energy per unit area and the ultimate strain less experimental support currently exists, although Körmeling observed the same tendencies in softening behaviour under high strain rates. For unloading a secant model without rate-dependence is used.
In a smeared crack approach we apply a decomposition of total strain into elastic strain $\boldsymbol{\varepsilon}_{co}$ and crack strain $\boldsymbol{\varepsilon}_{cr}$. Therefore the incremental stress-strain relation can be written as

$$\Delta\boldsymbol{\sigma} = \boldsymbol{D}_{co}(\Delta\boldsymbol{\varepsilon} - \Delta\boldsymbol{\varepsilon}_{cr}), \tag{4}$$

where the matrix $\boldsymbol{D}_{co}$ contains the instantaneous moduli of the concrete and $\Delta\boldsymbol{\varepsilon}_{cr}$ is the incremental crack strain. Generalising eq. (3) to two dimensions we obtain

$$\Delta\boldsymbol{\sigma} = \boldsymbol{D}_{cr}\,\Delta\boldsymbol{\varepsilon}_{cr} + \boldsymbol{M}\Delta\dot{\boldsymbol{\varepsilon}}_{cr}, \tag{5}$$

in which $\boldsymbol{D}_{cr} = \text{diag}\,[D_1, 0]$ and $\boldsymbol{M} = \text{diag}[M_1, 0]$. In other words only mode-I effects are considered. $\Delta\dot{\boldsymbol{\varepsilon}}_{cr}$ is the difference between the crack strain rates in the beginning and at the end of the time step respectively. Combination of eqs. (4) and (5) yields

$$\Delta\boldsymbol{\varepsilon}_{cr} = (\boldsymbol{D}_{cr} + \boldsymbol{D}_{co})^{-1}[\boldsymbol{D}_{co}\,\Delta\boldsymbol{\varepsilon} - \boldsymbol{M}\Delta\dot{\boldsymbol{\varepsilon}}_{cr}]. \tag{6}$$

This equation can be substituted in eq. (4), which gives the global constitutive equation:

$$\Delta\boldsymbol{\sigma} = \boldsymbol{D}_{co}[\boldsymbol{I} - (\boldsymbol{D}_{cr} + \boldsymbol{D}_{co})^{-1}\boldsymbol{D}_{co}]\Delta\boldsymbol{\varepsilon} + \boldsymbol{D}_{co}[\boldsymbol{D}_{cr} + \boldsymbol{D}_{co}]^{-1}\boldsymbol{M}\Delta\dot{\boldsymbol{\varepsilon}}_{cr}. \tag{7}$$

For the sake of simplicity only one crack has been considered in this derivation and the axes of the crack plane are assumed to be aligned with the global element axes. For a general treatment of the linear strain rate dependent model see Sluys (1991).

Next, we shall integrate eq. (7) over a finite time step Δt. In this derivation we define $\Delta \boldsymbol{\varepsilon}_{\mathrm{cr}}^{\mathrm{t}+\Delta \mathrm{t}}$ as the incremental crack strain in time interval $t \leq \tau \leq t + \Delta t$. By utilising the crack strain rate at the beginning of the time step $\dot{\boldsymbol{\varepsilon}}_{\mathrm{cr}}^{\mathrm{t}}$ and that at the end of the time step $\dot{\boldsymbol{\varepsilon}}_{\mathrm{cr}}^{\mathrm{t}+\Delta \mathrm{t}}$ the incremental crack strain is chosen according to

$$\Delta \boldsymbol{\varepsilon}_{\mathrm{cr}}^{\mathrm{t}+\Delta \mathrm{t}} = \left((1-\Theta)\dot{\boldsymbol{\varepsilon}}_{\mathrm{cr}}^{\mathrm{t}} + \Theta \dot{\boldsymbol{\varepsilon}}_{\mathrm{cr}}^{\mathrm{t}+\Delta \mathrm{t}}\right)\Delta t, \tag{8}$$

where Θ is an interpolation parameter for which $0 \leq \Theta \leq 1$. For $\Theta = 0$ we obtain the fully explicit Euler scheme. On the other hand $\Theta = 1$ gives a scheme that is fully implicit and the case in which $\Theta = \frac{1}{2}$ represents an implicit scheme according to the trapezoidal rule. From the definition of $\Delta \dot{\boldsymbol{\varepsilon}}_{\mathrm{cr}}$ we have

$$\Delta \dot{\boldsymbol{\varepsilon}}_{\mathrm{cr}}^{\mathrm{t}+\Delta \mathrm{t}} = \dot{\boldsymbol{\varepsilon}}_{\mathrm{cr}}^{\mathrm{t}+\Delta \mathrm{t}} + \dot{\boldsymbol{\varepsilon}}_{\mathrm{cr}}^{\mathrm{t}}, \tag{9}$$

which can be combined with eq. (8) to give

$$\Delta \dot{\boldsymbol{\varepsilon}}_{\mathrm{cr}}^{\mathrm{t}+\Delta \mathrm{t}} = \frac{1}{\Theta}\left(\frac{\Delta \boldsymbol{\varepsilon}_{\mathrm{cr}}^{\mathrm{t}+\Delta \mathrm{t}}}{\Delta t} - \dot{\boldsymbol{\varepsilon}}_{\mathrm{cr}}^{\mathrm{t}}\right). \tag{10}$$

We estimate $\dot{\boldsymbol{\varepsilon}}_{\mathrm{cr}}^{\mathrm{t}}$ by a central difference approximation:

$$\dot{\boldsymbol{\varepsilon}}_{\mathrm{cr}}^{\mathrm{t}} = \frac{1}{2}\left(\dot{\boldsymbol{\varepsilon}}_{\mathrm{cr}}^{\mathrm{t}-1/2\Delta \mathrm{t}} + \dot{\boldsymbol{\varepsilon}}_{\mathrm{cr}}^{\mathrm{t}+1/2\Delta \mathrm{t}}\right) = \frac{1}{2\Delta t}\left(\Delta \boldsymbol{\varepsilon}_{\mathrm{cr}}^{\mathrm{t}} + \Delta \boldsymbol{\varepsilon}_{\mathrm{cr}}^{\mathrm{t}+\Delta \mathrm{t}}\right). \tag{11}$$

By substituting eq. (11) into eq. (10) we obtain an expression for the incremental strain rate vector

$$\Delta \dot{\boldsymbol{\varepsilon}}_{\mathrm{cr}}^{\mathrm{t}+\Delta \mathrm{t}} = \frac{1}{2\Theta \Delta t}\left(\Delta \boldsymbol{\varepsilon}_{\mathrm{cr}}^{\mathrm{t}+\Delta \mathrm{t}} - \Delta \boldsymbol{\varepsilon}_{\mathrm{cr}}^{\mathrm{t}}\right). \tag{12}$$

Eq. (12) is now combined with eq. (7) to obtain the incremental constitutive relation

$$\Delta \boldsymbol{\sigma}^{\mathrm{t}+\Delta \mathrm{t}} = \boldsymbol{D}_{\tan} \Delta \boldsymbol{\varepsilon}^{\mathrm{t}+\Delta \mathrm{t}} - \Delta \boldsymbol{q}, \tag{13}$$

where

$$\boldsymbol{D}_{\tan} = \boldsymbol{D}_{\mathrm{co}}\left[\boldsymbol{I} - \left(\boldsymbol{D}_{\mathrm{cr}} + \boldsymbol{D}_{\mathrm{co}} + \frac{\boldsymbol{M}}{2\Theta \Delta t}\right)^{-1} \boldsymbol{D}_{\mathrm{co}}\right]$$

and

$$\Delta \boldsymbol{q} = \boldsymbol{D}_{\mathrm{co}}\left[\boldsymbol{D}_{\mathrm{cr}} + \boldsymbol{D}_{\mathrm{co}} + \frac{\boldsymbol{M}}{2\Theta \Delta t}\right]^{-1} \frac{\boldsymbol{M}}{2\Theta \Delta t} \Delta \boldsymbol{\varepsilon}_{\mathrm{cr}}^{\mathrm{t}}.$$

Matrix $\boldsymbol{D}_{\tan}$ is not determined only by material parameters since the time integration parameters Δt and Θ also appear. $\Delta \boldsymbol{q}$ can be considered as a pseudo-load vector. The material parameters can be grouped into a length scale parameter l via

$$l = \frac{M_1 c}{E}, \tag{14}$$

where c is the longitudinal wave velocity $\sqrt{E/\varrho}$ in which ϱ is the density. If the length

scale parameter vanishes due to a decreasing viscosity the rate-independent solid emerges as the limit of the rate-dependent model. In the foregoing it was said that the inclusion of rate dependence prevents the initial value problem from becoming elliptic. This can be proved by considering the quasi-linear system of equations

$$\sigma = f(\varepsilon_{cr}) + M_1 \frac{\partial v}{\partial x} - \frac{M_1}{E} \frac{\partial \sigma}{\partial t} \tag{15}$$

$$\frac{\partial \sigma}{\partial x} = \varrho \frac{\partial v}{\partial t}, \tag{16}$$

where the velocity v is the derivative of the displacement with respect to time. Combinning eqs. (15) and (16) results in the second order differential equation

$$\frac{\partial^2 v}{\partial x^2} - \frac{1}{c^2} \frac{\partial^2 v}{\partial t^2} - \frac{\varrho}{M_1} \frac{\partial v}{\partial t} = -\frac{1}{M_1} \frac{\partial f(\varepsilon_{cr})}{\partial x}. \tag{17}$$

The character of a partial differential equation is determined by the terms having the highest order. This means that eq. (17) is a hyperbolic equation with a source term which depends on the softening function. The characteristics of this system are real and have the physical meaning of a wave velocity. So, the problem remains well-posed and describes the localisation behaviour of the underlying physical material, as will be shown in the next section.

3 One-dimensional localisation problems

To investigate the performance of the rate-dependent crack model numerical simulations have been carried out for a one-dimensional bar in tension. Attention was focused on the influence of mesh spacing on the strain localisation in the bar and the wave reflection on cracked zones. The problem is sketched in Fig. 2: the magnitude of the impact load is taken as being 75% of the maximum tensile load in the static case, whilst the loading rate is determined by time span t_d. The bar has a length of 5 m and is divided into 10, 20, 40 and 80 elements respectively. Use has been made of eight-noded elements with a nine-point Gauss integration scheme. The longitudinal wave velocity $c = 1000$ m/s. If not specifically stated otherwise, the material parameters are as given in Fig. 1. The response of the bar is linearly elastic until the loading wave reaches the left boundary where reflection of the wave causes crack initiation. The material enters the softening regime and a localisation zone of intense straining occurs. The time integration of the field equations has been done with a Newmark scheme ($\beta = \frac{1}{4}, \gamma = \frac{1}{2}$).

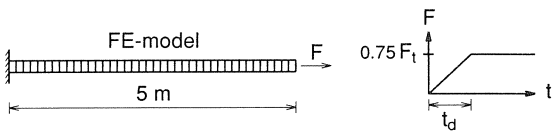

Fig. 2. Finite element model (40 elements) and time-load diagram.

3.1 *Rate-independent crack model*

The analyses with a rate-independent solid have been carried out to demonstrate the mesh-dependence of strain localisation and wave reflection. The comparison with the rate-dependent model is difficult because we cannot employ exactly the same softening diagram. A linear model is used with an ultimate strain equal to the peak strain which occurs in the localisation band of the rate-dependent analysis to be discussed next. This results in a softening modulus $D_1 = -1000$ N/mm^2. We consider a shock wave with a vertical stress front which corresponds to $t_d = 0$. The results for the different meshes are plotted in Fig. 3. Mesh sensitivity is obvious from the strain plots: strain localisation occurs in only one integration point which is the smallest possible zone. The results for the discretisations with 40 and 80 elements have not been plotted because at $t = 0.009$ s the bar has already failed. Instead, the results for a 5 element mesh are given. The stress plots show that the amount of wave reflection depends on the mesh: the more elements present, the larger the reduction in stress of the reflected wave. Furthermore, the energy dissipation decreases under mesh refinement and approaches the limiting case of failure without energy dissipation.

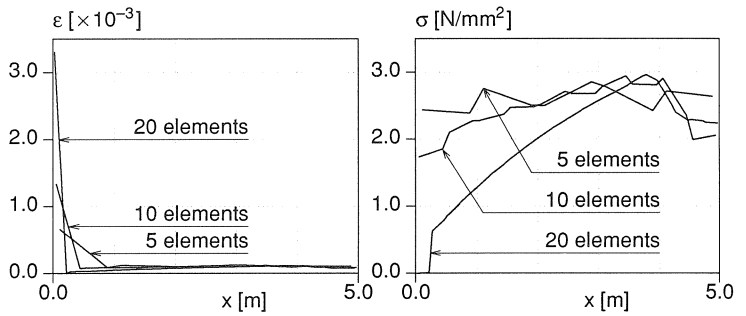

Fig. 3. Strain localisation (left) and stress distribution (right) along the bar at $t = 0.009$ s for three different meshes in a rate-independent solid.

3.2 *Rate-dependent crack model*

Rate dependence is applied according to the constitutive equation (13). It appears that the choice $\Theta = \frac{1}{2}$ for the interpolation parameter gives stable and accurate results, but that the time step Δt must be taken as smaller than $h/5c$, where h is the element size. This is a strong requirement that is caused by the sensitivity of the edge between the localisation zone and the elastically unloading remaining part of the bar. If the time step is taken as larger than $h/5c$ the strain profile is disturbed in these edge zones. Use of the reference material parameter set of par. 2 results in a length scale parameter $l = 400$ mm. The same loading pulse with $t_d = 0$ is applied. For the rate-dependent solid a localisation zone emerges that converges to a finite, constant band width upon mesh refinement. In Fig. 4 the strain localisation is plotted for different meshes to demonstrate the uniqueness of the solution. The coarse meshes (10 and 20 elements)

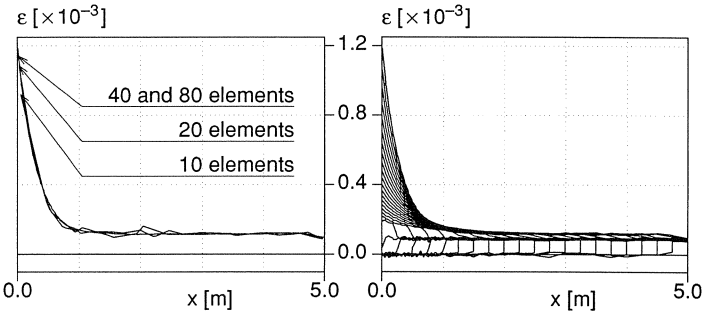

Fig. 4. Rate-dependent model with $t_d = 0$ s: Left: Strain profiles for different discretisations at $t = 0.01$ s. Right: Development of the localisation band (80 elements).

still deviate somewhat but the fine meshes (40 and 80 elements) give identical results, not only in the sense that the band width is constant but also that the energy dissipation is constant and the wave reflection pattern is mesh objective.

A second analysis has been carried out for a different loading pulse. In the time-load diagram the time span t_d is chosen as $2.5 \cdot 10^{-3}$ s. So, the loading pulse firstly increases linearly in time before it becomes constant. Again the effect of the inclusion of the length scale can be observed from the strain localisation plots in Fig. 5. Convergence to a unique solution with a finite localisation zone characterises the mesh independence. It is noted that the strain distribution in the localisation zone has a different shape for this loading case. In the previous analysis a sharp peak in the strain occurs at the left boundary, whereas in this analysis the strain profile is more uniformly distributed and has a lower peak value. This is due to the strain rate profile in the bar at the moment of cracking. In the previous analysis cracking is initiated in one point at the left boundary. From there the localisation zone extends in the direction of the reflected wave with a rapidly decreasing strain rate. In this analysis the static tensile strength is exceeded over a zone with a certain length (exact length = 833 mm). In this zone much lower and almost constant strain rates occur compared to the peak strain rate in the previous analysis.

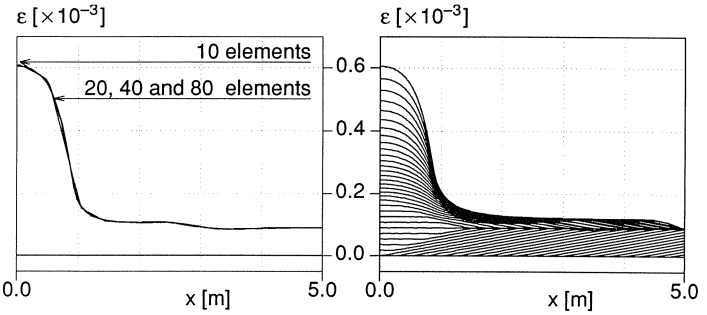

Fig. 5. Rate-dependent model with $t_d = 2.5 \cdot 10^{-3}$ s: Left: Strain profiles for diferent discretisations at $t = 0.0125$ s. Right: Development of the localisation band (80 elements).

Finally, the localisation band width has been analysed. Firstly the influence of the length scale parameter on the observed localisation width was investigated in an analysis with $t_d = 0$ by using three different values for l, namely 200, 400 and 600 mm. From the left plot of Fig. 6 it appears that the width of the localised zone is proportional to the length scale parameter. These results agree with the fact that the localisation zone vanishes when the length scale parameter approaches zero. A comparison of the results shown in Figs. 4 and 5 had already made it clear that the shape of the loading wave influences the strain rate distribution in the localisation zone and therefore also the localisation band width. This effect is shown in the right plot of Fig. 6 by taking three different values for the time span t_d in which the load is increased from zero to its maximum value.

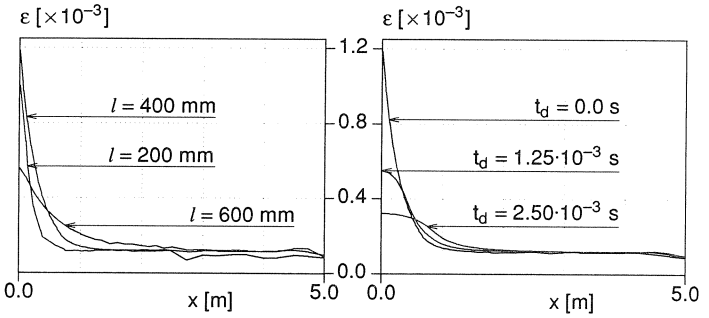

Fig. 6. Left: Variation of the length scale parameter. Note that for $l = 200$ mm the strain profile has been plotted at an earlier stage ($t = 0.0075$ s) than for $l = 400$ mm and $l = 600$ mm ($t = 0.010$ s). Right: Variation of the loading rate for a 40 element analysis ($t = 0.010$ s).

4 Impact tensile tests on notched specimens

In the Stevin Laboratory of Delft University of Technology impact tensile tests have been carried out on notched, prismatic concrete specimens (Fig. 7). A geometry with notches makes it possible to fix the failure plane and to measure the deformation inside as well as outside the fracture zone. The tests have been performed with the Split-Hopkinson bar apparatus by Weerheijm and Reinhardt (1989). The specimen is kept between an upper and a lower bar and the pulse is applied at the bottom of the experimental set-up. The main observations that have been reported are: the ultimate strength and the deformations inside and outside the fracture zone. The loading rate has been measured after the pulse passes the specimen and has been affected by the failure process and the geometry of the specimen.

Numerical analyses of the tests on specimens with a notch depth of 7 mm have been carried out earlier with a rate-independent crack model in order to demonstrate the mesh-sensitive behaviour and the influence of the structural response on the load-displacement data (Sluys 1989b, Sluys and De Borst 1990). In this type of experiment a pronounced rotation of the specimen occurs during failure, which may have been influenced by the experimental set-up. This rotation of the specimen was not found in

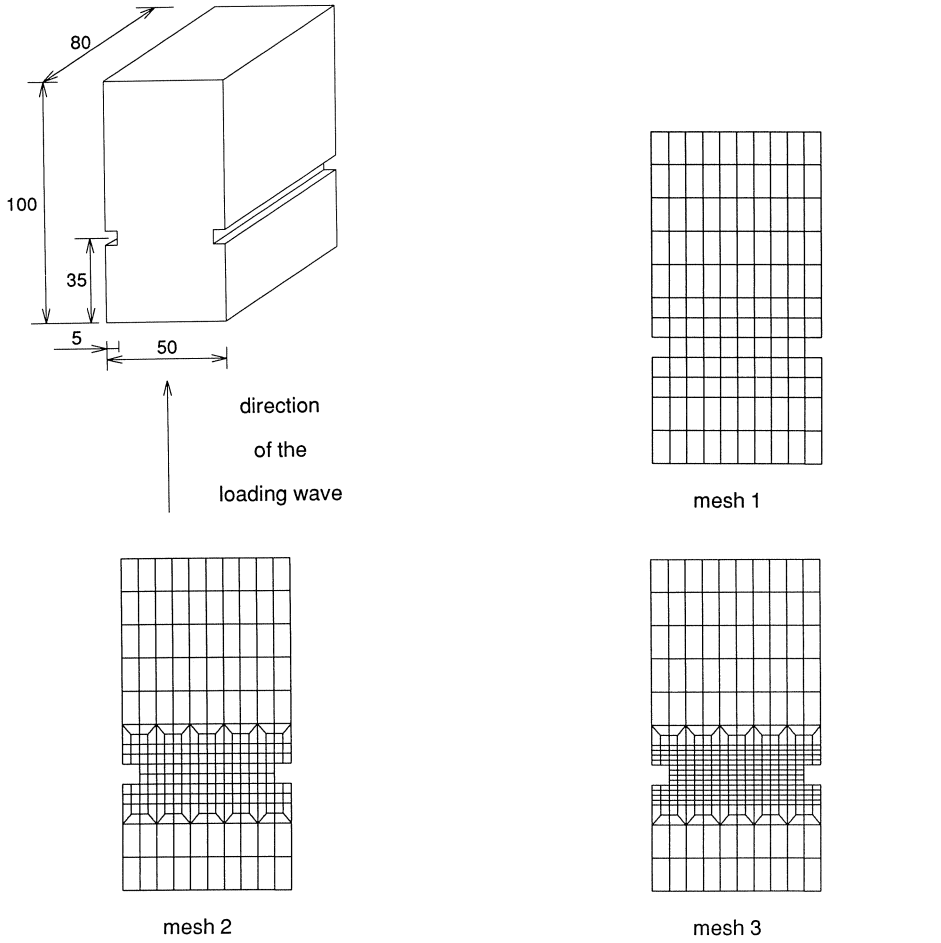

Fig. 7. Geometry of specimen (left) and finite element configurations with 1 (mesh 1), 2 (mesh 2) and 4 (mesh 3) rows of elements in the notched zone.

the numerical simulation. Because the rotation mechanism was less marked for the specimens with notches of 5 mm these tests were used for the analyses carried out with the rate-dependent fracture model. For the modelling of the Split-Hopkinson bar (height 11.2 m) the same discretisations as in the previous analyses (Sluys 1989b) have been adopted in which special boundary elements have been used to slow down the loading wave without undesirable reflections. For the specimen itself three finite element discretisations have been used (Fig. 7). For the different meshes we use one, two and four rows of elements in the notched section respectively. All numerical analyses have been performed under the condition of plane stress with quadrilateral elements with eight nodes and a nine-point Gauss integration. The analyses reported in this paper can be viewed as pilot calculations in which the material parameters

have been chosen as: $E = 40700$ N/mm^2, $D_1 = -2667$ N/mm^2, $M_1 = 0.08$ Ns/mm^2, $f_i = 4.0$ N/mm^2 and $\varrho = 2350$ kg/m^3. This material parameter set results in a length scale parameter $l = 8.2$ mm. In the analyses a section of 5×6 mm in front of the left notch was given a material imperfection in the sense that the tensile strength was reduced by 20%. By inserting an imperfection the possibility is offered of computing an asymmetric component of the solution.

The computational results differ markedly from the results obtained with the rate-independent crack model. Now, a localisation band occurs that is independent of the choice for the finite element discretisation. At the notches the very local stress concentration zones keep the band small but the width of the localisation band increases when the crack propagates to the centre of the specimen. This can be seen from the crack patterns in Fig. 8 for the three meshes at a time when the failure zone has developed

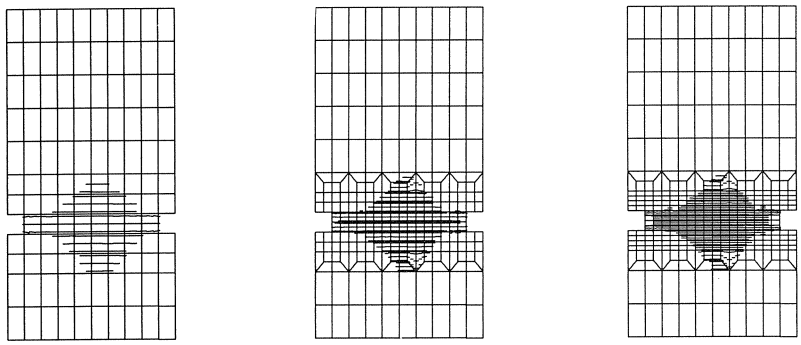

Fig. 8. Crack patterns at $t = 0.45 \cdot 10^{-3}$ s.

completely. Mesh objectivity can also be shown when the consumption of energy in the model is considered. From Fig. 9 it appears that the internal energy in the three configurations is more or less equal during the time of computation. The stress-deformation curves for the numerical analyses as well as for the experiment are plotted in Fig. 10, in which δ_{notch} represents the mean deformation over the left and the right notch and σ represents the vertical stress at the top of the specimen. Not only the mesh independence but also the similarity between numerical analysis and experiment is obvious. The development of the localisation band can be investigated in more detail if we consider the vertical strain in a relevant part of the specimen (Fig. 11). Cracking starts in the singular points at the upper and lower corner of the notches. Both cracks at the left notch first join and at a later stage split up into two separate localisation bands. So there remains an almost unstretched zone in the middle of the specimen. The same crack propagation process occurs at the right notch. The rotation during failure which is observed in the test is found to be less in the numerical simulation.

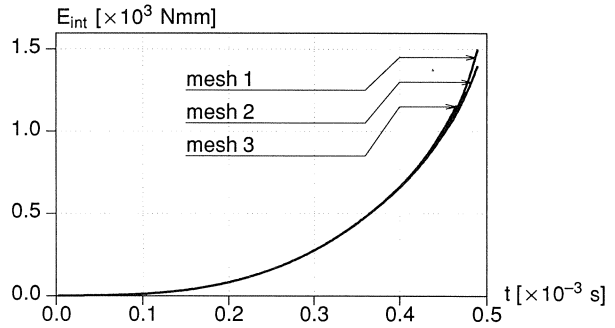

Fig. 9. Energy consumption in the model during the time of computation.

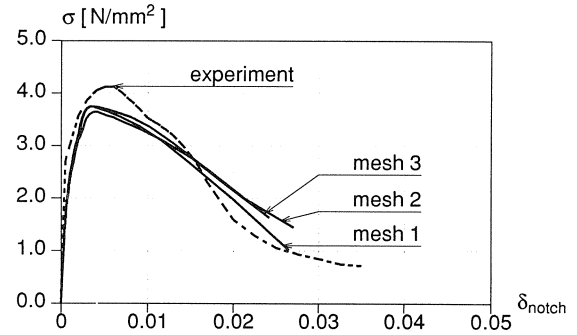

Fig. 10. Stress-deformation curve inside the fracture zone.

5 Concluding remarks

It has been demonstrated that numerical solutions for localisation problems are mesh-sensitive, show a spurious strain localisation behaviour and a disturbed wave reflection pattern when use is made of a rate-independent strain-softening model. Therefore a model has been proposed that includes a dependence on the strain rate. This prevents the initial value problem from becoming elliptic. A linear rate dependence is used in which the strain rate vector is integrated with an implicit algorithm. The model incorporates a length scale parameter which is necessary to overcome the mesh-sensitivity problem. One-dimensional numerical analyses have proved the mesh objectivity of the model with respect to the width of the localisation zone, the dissipation of energy and the wave reflection on the cracked zone. It appears that the width of the localisation zone is proportional to the length scale parameter. The mesh independence is also found in the pilot calculation of the tensile tests on notched specimens in which the solution for the failure zone deviates totally from the rate-independent solution.

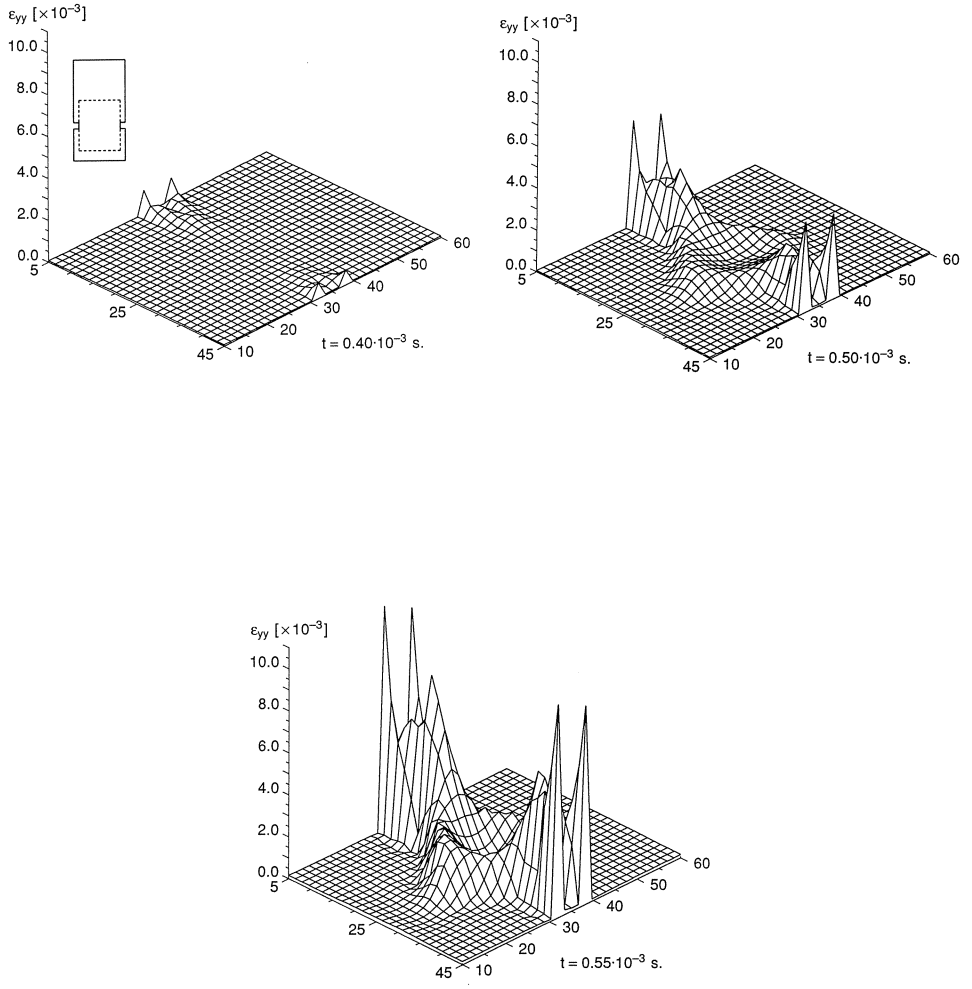

Fig. 11. Development of the vertical strain at several time steps (mesh 3).

Acknowledgements

The calculations described in this paper have been carried out using the DIANA finite element package of TNO Building and Construction Research. The authors acknowledge the stimulating discussions with J. Weerheijm on the experiments. This project is partially funded by the Prins Maurits Laboratory of TNO.

References

BAZANT, Z. P. and BELYTSCHKO, T. B. (1985), Wave propagation in a strain softening bar-exact solution. ASCE J. Engrg. Mech., 111(3), pp. 381–389.

DE BORST, R. and NAUTA, P. (1985), Non-orthogonal cracks in a smeared finite element model. Eng. Comput., 2(1), pp. 35–46.

DE BORST, R. (1990), Simulation of localisation using Cosserat theory, in Proc. 2nd Int. Conf. Computer Aided Analysis and Design of Concrete Structures, (eds N. Bićanić and H. A. Mang), Pineridge Press, Swansea, pp. 931–944.

DE BORST, R. and MÜHLHAUS, H.-B. (1991), Continuum models for discontinuous media, in Proc. Conf. on Fracture Processes in Brittle Disordered Materials, (eds. J. van Mier, J. G. Rots and A. Bakker), Chapman and Hall, London, pp. 601–618.

KÖRMELING, H. A. (1986), Strain rate and temperature behaviour of steel fibre concrete in tension Dissertation, Delft University of Technology, Delft, The Netherlands.

LASRY, D. and BELYTSCHKO, T. B. (1988), Localization limiters in transient problems. Int. J. Solids Structures, 24, pp. 581–597.

MÜHLHAUS, H.-B., DE BORST, R. and AIFANTIS E. C. (1991), Constitutive models and numerical analyses for inelastic materials with microstructure, in Proc. Seventh Conf. Int. Assoc. Comp. Methods and Advances in Geomechanics, (eds. G. Beer and J. R. Booker), Balkema, Rotterdam and Boston, pp. 377–386.

MÜHLHAUS, H.-B. and AIFANTIS, E. C. (1991), A variational principle for gradient plasticity. Int. J. Solids Structures, 28, pp. 845–857.

NEEDLEMAN, A. (1988). Material rate dependence and mesh sensitivity on localisation problems. Comp. Meth. Appl. Mech. Eng., 67, pp. 69–86.

PIJAUDIER-CABOT, G. and Bazant, Z. P. (1987), Nonlocal damage theory. ASCE J. Eng. Mech., 113, pp. 1512–1533.

READ, H. E. and HEGEMIER, G. A. (1984), Strain softening of rock, soil and concrete – A review article. Mech. of Mat., 3, pp. 271–294.

ROTS, J. G. (1988), Computational modeling of concrete fracture. Dissertation, Delft University of Technology, Delft, The Netherlands.

SANDLER, I. S. (1984), Strain softening for static and dynamic problems. Constitutive Equations – Macro and Computational Aspects – ASME, pp. 217–231.

SCHREYER, H. L. and CHEN, Z. (1986), One-dimensional softening with localization. J. Appl. Mech., 53, pp. 791–979.

SLUYS, L. J. (1989a), Strain softening under static and dynamic loading conditions. TU-Delft report, nr. 25.2-89-5-09.

SLUYS, L. J. (1989b), Numerical analyses of impact tensile tests on concrete. TU-Delft report, nr. 25.2-89-5-15.

SLUYS, L. J. and DE BORST, R. (1990), A numerical study of concrete fracture under impact loading, in Proc. Conf. Micromechanics of Failure of Quasi-Brittle Materials, (eds. S. P. Shah, S. E. Swartz and M. L. Wang), Elsevier Applied Science, London and New York, pp. 524–535.

SLUYS, L. J. (1990), Localisation in a Cosserat continuum under dynamic loading conditions. TU-Delft report, nr. 25.2-90-5-15.

SLUYS, L. J. (1991), Rate-dependent modelling for dynamic localisation. TU-Delft report, nr. 25.2-91-5-03.

WEERHEIJM, J. and REINHARDT, H. W. (1989), Concrete in impact tensile tests, in Proc. First Int. Conf. on Structures under Shock and Impact, Cambridge, Massachusetts.

WU, F. H. and FREUND, L. B. (1984), Deformation trapping due to thermoplastic instability in one-dimensional wave propagation. J. of Mech. Phys. Solids, 32, 2, pp. 119–132.

ZIELINSKI, A. J. (1982), Fracture of concrete and mortar under uniaxial impact tensile loading. Dissertation, Delft University of Technology, Delft, The Netherlands.